Journal of *Marine Science and Engineering*

MDPI

Article

Qualitative Study of the Transport of Microplastics in the Río de la Plata Estuary, Argentina, through Numerical Simulation

Alejandra Elisei Schicchi [1,*], Diego Moreira [2], Patricia Eisenberg [3] and Claudia G. Simionato [2]

[1] National Institute of Industrial Technology, Buenos Aires B1650WAB, Argentina
[2] Department of Atmospheric and Ocean Sciences (DCAO), Faculty of Exact and Natural Sciences, CONICET—Centro de Investigaciones del Mar y la Atmósfera (CIMA), Instituto Franco-Argentino de Estudios sobre el Clima y sus Impactos (IFAECI)—IRL 3351—CNRS-CONICET-IRD-UBA, University of Buenos Aires, Buenos Aires 1428, Argentina; moreira@cima.fcen.uba.ar (D.M.); simionato@cima.fcen.uba.ar (C.G.S.)
[3] Institute for Environmental Research and Engineering, 3iA, University of San Martín (USAM), Buenos Aires CP 1650, Argentina; peisenberg@unsam.edu.ar
* Correspondence: aelisei@inti.gob.ar

Abstract: Information about the sources, sinks, dynamics, and how environmental variables affect the transport of microplastics (MPs) from continental deposits to marine systems is still limited. Most of the knowledge about the distribution of plastic in the oceans comes from the use of numerical models to understand the routes of MPs moving in aquatic systems. The Río de la Plata (RdP) is an estuary located on the eastern coast of South America and is one of the most anthropized watercourses in the region. In this study, the trajectory of MPs in the RdP was examined through the implementation, for the first time for the region, of numerical simulation models. The impact of the estuary's hydrodynamic characteristics, winds, and MP morphological properties on their trajectory was investigated. The simulations produced demonstrated a high correlation between the hydrodynamics of the Río de la Plata and the trajectory of positively buoyant MPs. The wind was identified as a significant driving force in the simulation of MP motion dynamics. Modifications in the size of the MPs have more influence on the trajectory than their morphology. The results constitute an initial step toward understanding the dynamics of these emerging pollutants in one of South America's most important basins.

Keywords: microplastic; water pollution; numerical models; Río de la Plata

Citation: Elisei Schicchi, A.; Moreira, D.; Eisenberg, P.; Simionato, C.G. Qualitative Study of the Transport of Microplastics in the Río de la Plata Estuary, Argentina, through Numerical Simulation. *J. Mar. Sci. Eng.* **2023**, *11*, 2317. https://doi.org/10.3390/jmse11122317

Academic Editors: Christophe Maes and Bruno Sainte-Rose

Received: 27 October 2023
Revised: 29 November 2023
Accepted: 2 December 2023
Published: 7 December 2023

1. Introduction

Microplastics (MPs) are ubiquitous on a global scale, infiltrating every corner of the planet, from the Antarctic currents to the Arctic seafloor [1]. Recognized by the United Nations Environment Program as a pressing global pollution concern [2], marine ecosystems serve as significant repositories for MPs contamination, with an estimated 5.25 trillion plastic pieces adrift in the world's oceans. MPs infiltrate marine environments through sources such as surface runoff, aquaculture, and fisheries [3], of which around 75–80% come from land-based plastics [4]. Additional inputs arise from aquatic activities, including fishing nets [5].

Once in the marine environment, plastics persist for years. They undergo fragmentation due to photochemical and mechanical processes, resulting in the formation of MPs [6]. These environments also invite microbial colonization of MPs surfaces, promoting biofilm development [7]. This biofilm not only alters MPs density but also harbors human pathogens [7] and enhances the ability of MPs to accumulate persistent organic pollutants, heavy metals, and even antibiotics [3]. Due to their small size, MPs are bioavailable throughout the food web, leading to ingestion by various organisms and subsequent transport to distant regions [8]. The ingestion of MPs can result in issues ranging from

false satiation and mechanical damage to organism morbidity and mortality [2], while they may also potentially act as carriers of chemical pollutants [9] and cause toxicity via various mechanisms [10]. In addition, MPs enter the human body through food consumption, with traces found in blood, placenta, lungs, and feces [11]. Given their ubiquity, understanding MPs generation, flow-retention dynamics, origin–trajectory relationships, and deposition patterns is crucial [2]. Given that empirical data are scarce, understanding how plastic is distributed in the oceans relies primarily on numerical simulations [12]. There is limited understanding of the complex movements that are required to formulate effective management strategies, especially in coastal regions [13]. Numerical modeling helps to elucidate the "why", "where", and "how" of plastic entry into aquatic systems, enabling better comprehension of its impact on aquatic environments and biodiversity [14]. In the simulation of plastic transport, two principal approaches exist: the Eulerian framework, commonly used in sediment studies, and the Lagrangian framework [12]. Lagrangian simulations employ pre-calculated Eulerian velocity data, derived from observations or models, to compute virtual particle paths by integrating the varying velocity field over time [12]. The Lagrangian approach is based on the introduction of virtual particles freely moving through the hydrodynamic field simulated by ocean circulation models. It is most commonly used to study the transport of marine debris, including MPs [12,15,16] at both global and regional scales [9,17–20]. In parallel, experimental exercises have been carried out to track the position of the plastic debris by post-processing images taken by a video camera, as another way of studying this problem, helping to validate numerical model results. These experimental measurements demonstrate that wave-induced Lagrangian drift of plastic particles in intermediate water depths is strongly influenced by particle size and density, causing particles to float or sink for relative densities lower and higher than water [21]. Floating particles remain at the surface due to buoyancy, and there is no evidence of any other influence of particle inertia on the net drift. Non-suspended particles move close to the bottom with lower velocities than the movement of suspended particles near the surface [21]. The motion of floating particles is affected solely by wave orbital motion, whereas non-floating particles at the bottom of the flume are predominantly due to characteristics of the wave orbital motion at the bed [22]. Also, experimental measurements of beaching times for buoyant microplastic particles released have shown that all particles were transported in the onshore direction, eventually becoming beached [22]. In Passalacqua et al. [23], the transport of particles of nylon was investigated under different hydrodynamic conditions by processing video frames using computer vision techniques for the detection and analysis of connected pixels. The results showed that blob analysis is a useful technique for studying the movements of sets of non-buoyant plastic particles until they fall into the breaking zone; they are then mobilized out of the camera frame.

The track marine plastic debris (TrackMPD) model, based on the particle tracking on analysis toolbox (PaTATO) framework, facilitates 3D transport modeling of MP marine debris [24]. The TrackMPD stands out itself by its capacity to integrate a particular algorithm for calculating settling velocities of spherical and cylindrical particles in contrast to other Lagrangian models [24]. This approach has been effectively implemented in several areas of the world ocean. In Jervis Bay, the application of TrackMPD resulted in accurate estimation and prediction of marine plastic debris sources [24]. In the Yalu River estuary, the tracker was used to examine sedimentation due to land reclamation impacts [25]. The study of MPs contamination faces challenges due to limited access to quantitative data [26], especially in developing areas such as Argentina, where high costs hinder MPs collection efforts. This work is set in the Río de la Plata Estuary (RdP), which drains the waters of the world's fifth-largest fluvial basin [27] Also, RdP ranks second in South America in terms of drainage area and discharge flow rate [28]. Stretching across urban and industrial landscapes with major cities in Argentina and Uruguay along its margins, the RdP provides essential water supply to approximately 15 million people [27]. Despite its importance, observations of MPs in the RdP are still scarce. Pazos et al. (2021) [29] recorded monthly MPs presence over a year in a coastal area of the RdP, revealing February as the peak month

with the highest MPs concentration (110 MPs m^{-3}) in water and April (613 MPs m^{-2}) in sediments. Nevertheless, considerable knowledge gaps persist. This gap extends to nearby regions, as exemplified by Arias et al. (2019) [30], who found MPs in the gastrointestinal tract of commercial fish species in Bahía Blanca estuary, where 48.9% were fibers and 30.6% pellets. The purpose of this study is to conduct an initial exploration of MPs dynamics in the RdP using numerical simulations. The TrackMPD_v.1 software will be used to identify and evaluate the effect of hydrodynamic forces on MPs transport, assess path changes resulting from morphological properties (type and size), and analyze changes in MPs trajectories with varying wind speeds and directions. Our simulation, which necessitates simplifications in hydrodynamic modeling and consideration of MPs properties, represents a fundamental advancement in understanding the motion of MPs in the RdP.

Study Area

The RdP spans between 34° and 36° S, and 55° and 58° W and constitutes the border between Argentina and Uruguay. It has a northwest to southeast orientation and a surface area of 35,500 km^2 (Figure 1). The main characteristic is its shallowness (on average, 10 m) and funnel-shaped morphology. It is 327 km long, 40 km wide at its head, and 227 km wide at its mouth [27,31]. The RdP is a fluvial-marine environment, formed by the confluence of two of the most relevant rivers in South America, Paraná and Uruguay, discharging their waters into the Atlantic Ocean [32,33]. In the confluence between the strong discharge of the fluvial waters with the marine waters, an extensive mixing zone of mesohaline characteristics is generated [27]. It is a semi-permanent feature of the region [34]. Based on its geomorphological and dynamic characteristics, the RdP has been divided into three regions as described below [35–37].

Figure 1. Río de la Plata estuary and principal geographic locations. MODIS color image. (**a**) Upper region RdP, (**b**) intermediate region RdP, (**c**) outer region RdP.

Upper RdP: From the mouth of the tributary rivers to the imaginary line joining Punta Lara (Argentina) and Colonia del Sacramento (Uruguay), with fluvial waters and an average depth of less than 5 m.

Intermediate RdP: From the Punta Lara–Colonia de Sacramento line to the Punta Piedras–Montevideo line, with fluvial features, shallow sandbanks, and a depth of between 5 to 10 m.

Outer RdP: From Punta Piedras–Montevideo to Punta Rasa–Punta del Este, it is the deepest area with values of 15 to 20 m and mixohaline waters.

Water within the estuary is transported outwards. Its circulation is strongly influenced by bathymetry, the Earth's rotation, continental discharge, tide, and wind [37]. This circulation affects the mean sea level and determines the net mass transport. In the upper and intermediate regions, the circulation is barotropic, dominated mainly by the discharge of tributary rivers (Figure 2b), but also by the tides and winds (Figure 3). The water flow is concentrated along the deeper north and intermediate channels, and as the freshwater plume reaches the central part, the Coriolis effect due to the Earth's rotation causes the mass transport to be directed to the north. The circulation generated by the water mass transport is enhanced in high discharges and decreases accordingly in low discharges while maintaining the circulation pattern [38]. In the outer region the circulation becomes baroclinic, due to the density gradient produced by the encounter of river water with saline seawater [39,40]. Due to the shallow depth of the RdP, the currents in this region rapidly respond to winds, in particular to their direction, within 3 to 9 h [41]. The vertical structure of the currents can be explained in two modes or patterns. Winds with a dominant component perpendicular to the axis of the estuary (SW-NE) induce currents that decay vertically from the upper to the lower levels; this characteristic is a consequence of the geometry and bathymetry of the estuary [28]. Meanwhile, a wind component parallel to the axis of the RdP (NW-SE) produces a current reversal pattern, with an outflow of water mass in the upper layer and an inflow of water mass in the layers near the bottom of the river [37].

Table 1. Initial location for the simulation of MPs trajectories in the TrackMPD (Figure 2a).

MPs	Location: Lon, Lat	Reference
MP1	58.3° W, 34.3° S	Playa Honda, influenced by the tributary rivers' discharge (Uruguay and Paraná Guazú-Bravo).
MP2	58.3° W, 34.5° S	Playa Honda, influenced by the tributary rivers' discharge (Uruguay and Paraná Guazú-Bravo).
MP3	58.1° W, 34.68° S	Berazategui, near the plant of water effluent treatment (AySA).
MP4	57.88° W, 34.52° S	Near Colonia del Sacramento.

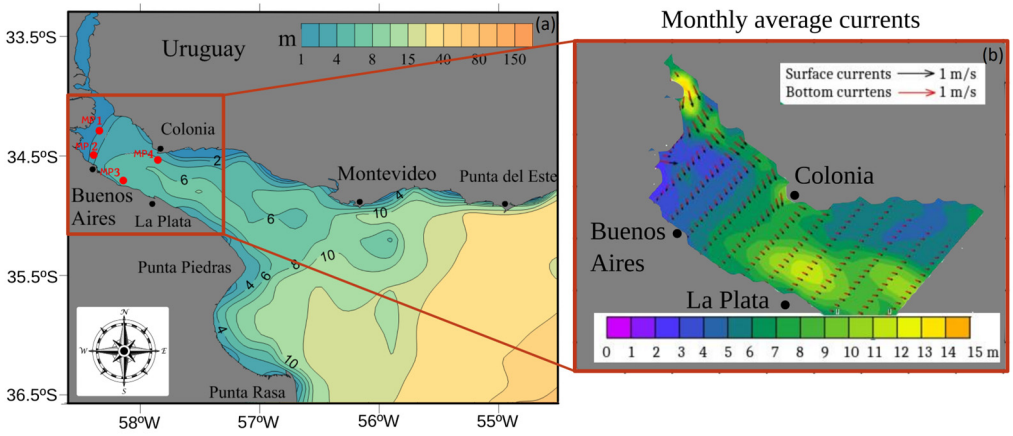

Figure 2. (**a**) Initial location chosen for MPs trajectories simulation (Table 1) and bathymetry of the Río de la Plata (in m). (**b**) Monthly average currents (m s^{-1}) near the surface (black arrows) and near the bottom (red arrow) indicating the mean flow pattern, over bathymetry (m).

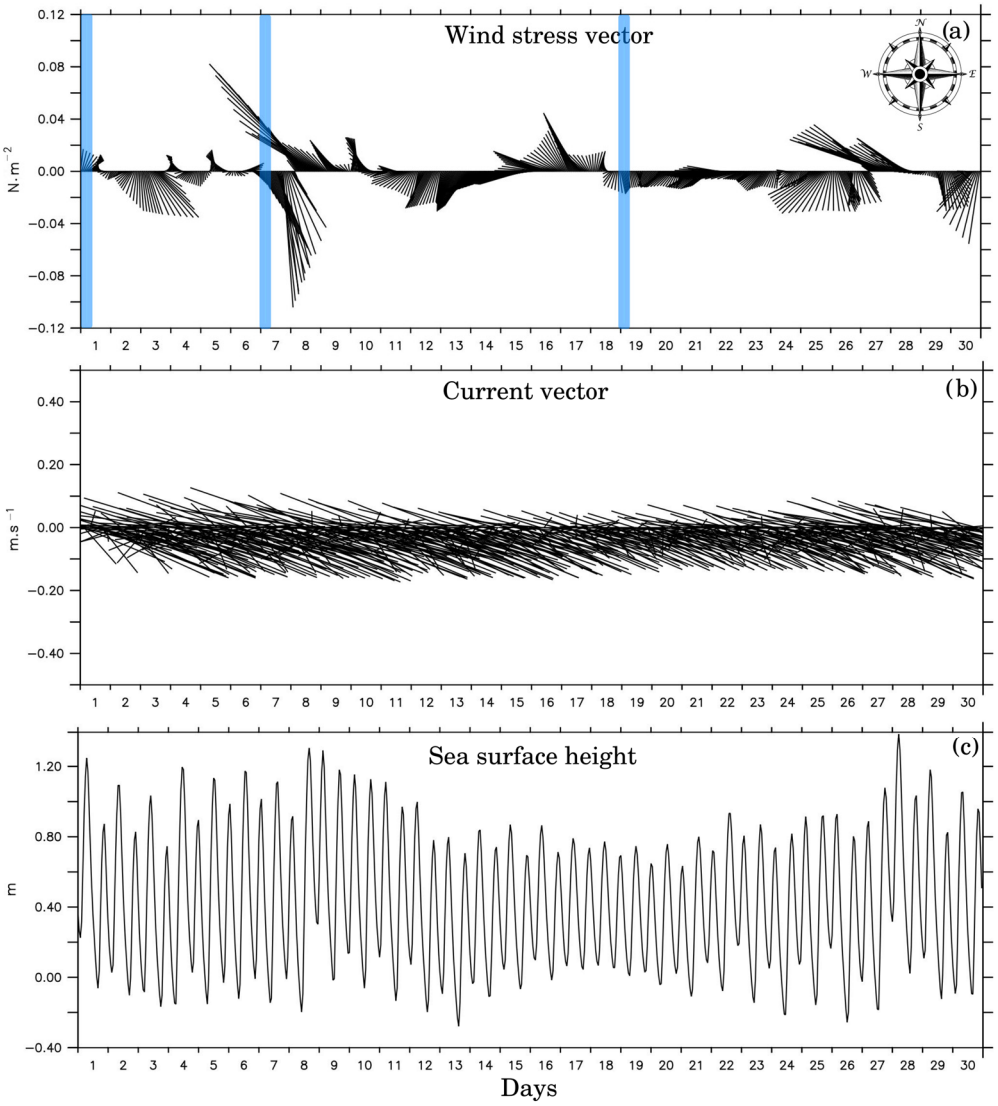

Figure 3. (**a**) Wind stress vector (N m^{-2}) for the modelated month. The light blue bars show at which time of the month the simulation was initialized. The first period starts on the first of the month, the second on the 7th, and the third on the 19th. All three end on the 30th of the chosen month. (**b**) Current vector, (**c**) surface height for a site in the upper RdP (34.36° S, 58.29° W).

The total average flow is about 23,200 m^3 s^{-1}, with peaks of 90,000 m^3 s^{-1} and troughs of 8000 m^3 s^{-1} [42,43]. Freshwater in the RdP comes from several tributaries, although the two most important are the Uruguay and Paraná Rivers (Figure 1), which account for more than 97% of the water discharged to the RdP. The largest flow (around 70%) is contributed by the Paraná River, with two main branches: the Paraná Guazú-Bravo with 77% of the water transport, and the Paraná de las Palmas with 23% of the remaining flow [36,43]. The Matanza-Riachuelo Basin is considered among the most polluted rivers in Latin America and drains directly into the RdP [44]. The Lujan River joins the RdP estuary close to the Paraná de las Palmas; it transports high concentrations of a wide range of contaminants from industrial activities and urban wastewaters [45].

The RdP has a microtidal astronomical regime, characterized by diurnal inequalities and important differences between consecutive high tides/low tides. The tidal energy flow enters through the SE sector of the mouth, propagating from S to N with higher amplitudes toward the coast and decreasing toward the interior of the estuary [41], behaving as a Kelvin wave forced at the shelf. The topography of the estuary modifies the wave as it propagates along the estuary, reducing the celerity and wavelength and causing the tidal

wave to decay due to the bottom friction [27]. The semidiurnal lunar component (M2) is the most significant for the system [38]; it is characterized by two high tides and two low tides during the lunar day, with very little difference in height between them, as the semidiurnal tide overlaps the diurnal tide [38]. The amplitude of this component reaches 0.65 m on Samborombón Bay and is reduced to 0.27 m in Buenos Aires [27]. Wind affects the dynamics at all scales in the RdP, being the main forcing agent of the circulation [28,37,46]. Through shear stress, wind modifies the propagation velocity of the tidal wave and the degree of vertical mixing and generates waves, displacing significant volumes of water [28]. The general circulation of the atmosphere in the area is controlled by the influence of the South Atlantic semi-permanent high-pressure system [47]. The anti-clockwise circulation advects warm and humid air from subtropical regions over the estuary [47]. On the other hand, cold fronts arrive from the south with a period of 4 days associated with convective storms called "Pamperos". This way, the area is characterized by the alternation of winds from NE to SW, with intervals of a few days [28,48,49]. Due to the general orientation of the RdP (NW-SE) and its shallow depth, only wind waves propagating from the SE sector can reach the interior of the estuary. Therefore, in the upper zone, wind waves are mostly locally generated [50]. The most frequent wave period range is around 3–4 s, with significant heights between 0.20 and 0.60 m [34]. Long-period waves from the deep waters of the Atlantic Ocean are damped and break as they enter inside the RdP [50].

2. Methods

2.1. Numerical Model

2.1.1. Hydrodynamic Simulation

The modular structure of TrackMPD involves the configuration of three initial data modules that allow the user to carry out simulations. The first module involves the integration of hydrodynamic data specific to the study area. This includes fixed parameters such as domain (area covered, number of grid points, resolution), bathymetry (depth), and number of vertical layers (σ, sigma vertical layers). Additionally, time-varying parameters including current speeds (u, zonal, and v, meridional velocities) and free surface elevation (xe) are essential components. These conditions were established using results from the model for applications at a regional scale (MARS) [51], developed by the Dynamics of the Coastal Environment Department (DYNECO) at the French Research Institute for the Exploitation of the Sea (IFREMER). Designed for coastal regions, MARS comprehends processes spanning diverse spatio-temporal scales, applicable to environments such as lagoons, beaches, bays, estuaries, continental shelves, and open oceans [51,52], effectively describing timescales ranging from hours to decades. The MARS model has been implemented, calibrated, and validated for the study area described above [34,46,53–56]. It operates within two nested domains. The largest, with lower resolution, covers the southwestern region of the South Atlantic Ocean from 69.35 to 45.5° W and 25.5 to 54.8° S; the resolutions are of 0.1° in latitude (~10 km) and 0.15° in longitude (~12 km), with one vertical layer. This model is used to provide boundary conditions to the smaller scale/higher resolution model. This latter domain, spanning from 32.9 to 38.139° S and 60.67 to 50.62° W, is tailored to the RdP and its adjacent shelf, employing a horizontal resolution of 0.027°(~3 km) and 10 sigma layers in the vertical to accurately represent study site vertical structure.

TrackMPD employed results from the second domain. Currents were sourced from MARS model outputs, necessitating the configuration of core drivers in the RdP: continental discharge, tide, wind, and waves. Data on continental water discharge from key tributaries, namely Paraná Guazú, Paraná de las Palmas, and Uruguay, were obtained from the "Sistema Nacional de Información Hídrica de la Nación" (accessed on 1 October 2022) and daily discharge estimates from the National Water Institute (INA, accessed on 1 October 2022). Considering their relevance to urban pollution contribution [27,57], discharge data from the Luján and Riachuelo rivers were also integrated. The resultant mean water discharge value amounted to 26,567 $m^3\ s^{-1}$, marginally surpassing historical averages reported in other studies [42,43,58].

2.1.2. Tracking Model

The trajectories of the MPs were determined by implementing the numerical model TrackMPD, which takes a comprehensive 3D approach that includes various physical processes and MPs behavior, depending on their dynamic properties. This approach distinguishes TrackMPD from other numerical models, which treat the MPs as neutral particles traversing the surface layers, neglecting their dynamic properties and adopting a two-dimensional approach [24]. TrackMPD's potential lies in its flexibility to incorporate velocity currents in a variety of formats and to extend the Lagrangian advection-diffusion model to include realistic particle behavior such as windage, beaching, degradation, and more [24]. Equation (1) represents the horizontal position (X) of a particle at time $t + \Delta t$ in the TrackMPD [25]:

$$X(t + \Delta t) = X(t) + U\Delta t + R\sqrt{2K_h\Delta t} \quad (1)$$

where $U = (u, v)$ is the horizontal current vector, K_h the diffusion coefficient (1 m^2 s^{-1}), and R is a random number generated per time step with an average and standard deviation from 0 to 1.

The vertical position (Z) at time $t + \Delta t$ is depicted by Equation (2):

$$Z(t + \Delta t) = Z(t) + w(t)\Delta t \quad (2)$$

where $Z(t)$ is the original vertical location of the particle at time t. Furthermore, Equation (3) provides the particles's vertical velocity:

$$w(t) = w(t) - w_s(t) + \frac{R\sqrt{2K_v\Delta t}}{\Delta t} \quad (3)$$

where w is the vertical velocity, w_s settling velocity and K_v is a vertical diffusion coefficient (1×10^{-5} m^2 s^{-1}). Drawing from recent experimental research, TrackMPD predetermines specific MPs behaviors, each defined by physical properties (density, shape, and size). For the purpose of this study, as a first approach, and to evaluate a simplified simulation, the "beaching" option was chosen, while the "re-suspension" option was excluded. The "beaching" approach implies that MPs reaching the coast do not re-enter the system and remain retained in the area. Conversely, "re-suspension" suggests that MPs settling on the RdP floor are trapped there. Our study uses behavior B1, corresponding to MPs with a density lower than 1 g dm^{-3} with w_s = 0, and behavior B3, polymers with a density greater than 1 g dm^{-3}, and allows the geometry to be specified [24]. For B1, the polymer density is the only input, while for B3 the size and shape of the MPs are also required. Biofouling, degradation, and biofilm formation are not considered in either behavior. The settling velocity for the B3 behavior is governed by Equations (4) and (5), depending on the particle shape.

The B3 behavior establishes the settling velocity as follows.

- For sphere

$$w_s = \frac{v}{2R}\, {d_*}^3 \left(38.1 + 0.93\, {d_*}^{\frac{12}{7}}\right)^{-7/8} \quad (4)$$

- For cylinders

$$w_s = \frac{\pi}{2}\frac{1}{v}\,\frac{(\rho_p - \rho_w)}{\rho_w}\,\frac{2\,RL}{55.238\,L + 12.691} \quad (5)$$

d_* is the dimensionless particle diameter ($d_* = 2R\left(g\left(\rho_p - \rho_w\right)/\rho_w v^2\right)^{1/3}$), ρ_p the particle density, ρ_w the water density (same units as ρ_p), v te water kinematic viscosity (10^{-6} m^2 s^{-1}), g the gravity acceleration (m s^{-2}), R radius (m), L (m).

Throughout this work, particles were released at the water surface in all simulations. To initiate MPs simulations, representative regions of the river were selected, with emphasis

on anthropogenic areas of substantial impact. Four points were chosen, as outlined in Table 1 and depicted in Figure 2a. These locations include points close to the tributary river mouths, the Buenos Aires city coast, urban regions contributing to anthropogenic pollution, and close to Colonia del Sacramento. It was decided not to release the MPs in positions close to the coast to avoid them, due to hydrodynamic effects, from being stranded there in a short time.

2.2. Model Configuration

2.2.1. Hydrodynamic Effects

In order to assess the impact of each forcing factor (continental discharge, tide, wind, and waves) on the trajectory of MPs, four simulations were conducted. These simulations will be referred to as "Hydrodynamic Cases." In each case, the forcing factors were introduced one at a time and varied in each hourly model step, as did the actual system conditions. In this way, the complexity of the simulation was gradually increased. Case I was run with continental discharge only; Case II was run again, adding the tides to the liquid discharge. The simulation was repeated with Case III adding the wind effect to the previous run. Finally, a real simulation was run with all active forcings (continental discharge + tide + wind + waves). For the trajectory simulations, the B1 behavior was selected. The user defines the polymer density as the only input parameter associated with plastic properties, without considering morphology or size. This behavior is restricted to plastics with density values less or equal to 1 g cm^{-3}. It is the simplest behavior of TrackMPD, allowing us to concentrate on how the estuary's hydrodynamics influence MPs trajectories by working with buoyant particles. The "re-suspension" option was excluded, and the "beaching" option was also chosen, so the test ends when MPs reach the coast. For these simulations, polypropylene (PP) was selected as the polymer. PP has a density of 0.84 g cm^{-3} [59]. The selection of this material is based on two primary reasons. Firstly, PP constitutes 19.2% of the annual global plastic production, primarily used for manufacturing containers and packaging for various items [60]. Additionally, according to Rodriguez et al. (2020) [61], 70% of plastics collected on Uruguayan coasts were identified as PP. They observed the highest density mean concentration of 292 items m^{-2} at one of the distant sites from the urban center of origin, suggesting that marine influences play a crucial role in plastic distribution. Moreover, the type of plastic found (171 pellets m^{-2}) indicated a prevalence of marine inputs.

The TrackMPD simulations cover a period of 30 days, as this duration represents the estuarine flushing time of the RdP [38,39,57,62]. The time step for current velocities (u, v) and free sea surface elevation (xe) was set at 1 h intervals. For these simulations, the water density value was predetermined by the TrackMPD model, maintaining a constant value of 1 g cm^{-3}, due to the fact that the upper and intermediate RdP are not influenced by the salt wedge located in the intermediate-exterior estuary [39]. The current speeds and sea surface height were obtained from the MARS model for one entire month and run in the TrackMPD simulations. These MARS solutions were analyzed in previous works by [46,56,62].

2.2.2. Dependence on Winds

Since winds have a substantial impact as a forcing agent on the water column in the RdP [28], and in order to understand the wind's effect on the simulation of MPs trajectories, the month of the run was partitioned into three time periods (Figure 3a).

The selection of the three periods was based on the wind speeds recorded during the chosen month. As can be seen in Figure 3a, the wind stress $(\tau_{sx}, \tau_{sy}) = \rho_a C d_s \sqrt{({u_{wnd}}^2 + {v_{wnd}}^2)}$ (u_{wnd}, v_{wnd}) where (τ_{sx}, τ_{sy}) are the wind stresses on the surface in zonal and meridional directions (around 0.01 and 0.005 N m^{-2}, respectively). During the first days of the month, the winds were weak and became stronger from the 7th day onwards. The first 7 days were covered by simulation W-I starting on the first day of the month with a period of 30 days. Simulation W-II starts on the 7th, with the first 4–5 days of strong winds, shifting from north-northwest to southwest directions. Finally, simulation W-III starts from the

19th to the 30th with calm conditions. The time step for all the simulations was one hour and was performed under the same hydrodynamic conditions (Case IV), behavior (B1), and PP material, with the "beaching" option and "re-suspension" option excluded. These conditions were chosen to highlight the importance of wind effects within the complicated RdP hydrodynamics by assuming a calm period alongside complex hydrodynamic scenarios. Figure 3b, correspond to the hydrodynamic conditions near the mouth of the RdP, in the upper RdP at coordinates latitude: 34.36° S, longitude: 58.29° W. Figure 3b shows the current vector over the month (vertical average) with south-southeast main direction, $U = 0.15$ m s^{-1} (zonal velocity) and $V = -0.1$ m s^{-1} (meridional velocity). Figure 3c shows the sea surface height for the same site where the effect of the tide can be appreciated, and the effect of the wind increasing the level at moments of greatest intensity and SE direction (7th and 27th). This positive storm surge effect is characteristic of the estuary and is called "sudestada".

2.2.3. Effect of Morphology

To assess the morphology of MPs within trajectories, the B3 behavior of TrackMPD was selected for a new series of simulations. This choice was founded on the capability to alter the geometry of MPs without introducing additional variables to the system, such as degradation or biofilm formation. The simulation was conducted using polystyrene (PS). The tabulated density of PS ranges from 1.04 to 1.07 g cm^{-3} [59]. For this study, a density of 1.04 g cm^{-3} was chosen for both shapes and sizes. PS constitutes 10% of the world's plastic production [60]. In construction, where weight reduction of structures is crucial, PS beads are often used in lightweight concrete, primarily for housing and building components. Although PS does not exist in a fiber form, considering density alone, it exhibits similar bibliographic density to some textile polyamides like Nylon Qiana (1.04 g cm^{-3}) and the more well-known Nylon 6.6 (1.14 g cm^{-3}).

Two geometries were examined: spherical and cylindrical (to mimic fibers), with two sizes chosen for each. For spheres, radii of 150 µm (according to Equation (4), $w_s = 103 \times 10^{-5}$ m s^{-1}) and 10 µm ($w_s = 0.5 \times 10^{-5}$ m s^{-1}) were selected. For cylindrical shapes, a radius of 150 µm with a length of 3000 µm (according to Equation (5), $w_s = 439 \times 10^{-5}$ m s^{-1}) and a size of 10 µm radius with 200 µm length ($w_s = 1.98 \times 10^{-5}$ m s^{-1}) were employed. These dimensions and geometries were adopted based on the studies by Pazos et al. (2021) [29] where almost 20% of the discovered plastics fell within the 500–100 µm size range, and the work of Ender et al. (2015) [59], which simulated spheres ranging from 1000 to 10 mm. All the simulations ended when MPs reached the coast option, and the "re-suspension" option was also excluded.

3. Results

3.1. Hydrodynamic Simulation Cases

3.1.1. Hydrodynamic Case I: Effect of the Continental Discharge

The four released MPs were primarily influenced by the continental discharge from tributaries within the estuary (Figure 4a). MP1, released at the mouth of the Uruguay and Paraná Guazú-Bravo tributaries, exhibited the strongest response to the discharge. It followed the longest trajectory among the group, almost reaching La Plata City. The time taken for MP1 to reach the coast was relatively short, approximately 70 h. In the absence of other driving forces, MP1 moved swiftly in an almost straight path toward the outer region of the RdP. MP2 moved southward and reached the coastline within 40 h, near the city of Buenos Aires. MP3, located close to the northern Punta Lara coast, displayed a trajectory roughly parallel to the estuary's axis, arriving at the southern coast in 35 h. On the other hand, MP4, released near Colonia del Sacramento along the northern RdP coast, moved southeastwards and reached the coast in about 65 h, indicating the occurrence of robust outflow-generated currents. Overall, the motion patterns of all MPs were aligned with the barotropic circulation prevalent in the upper section of the estuary.

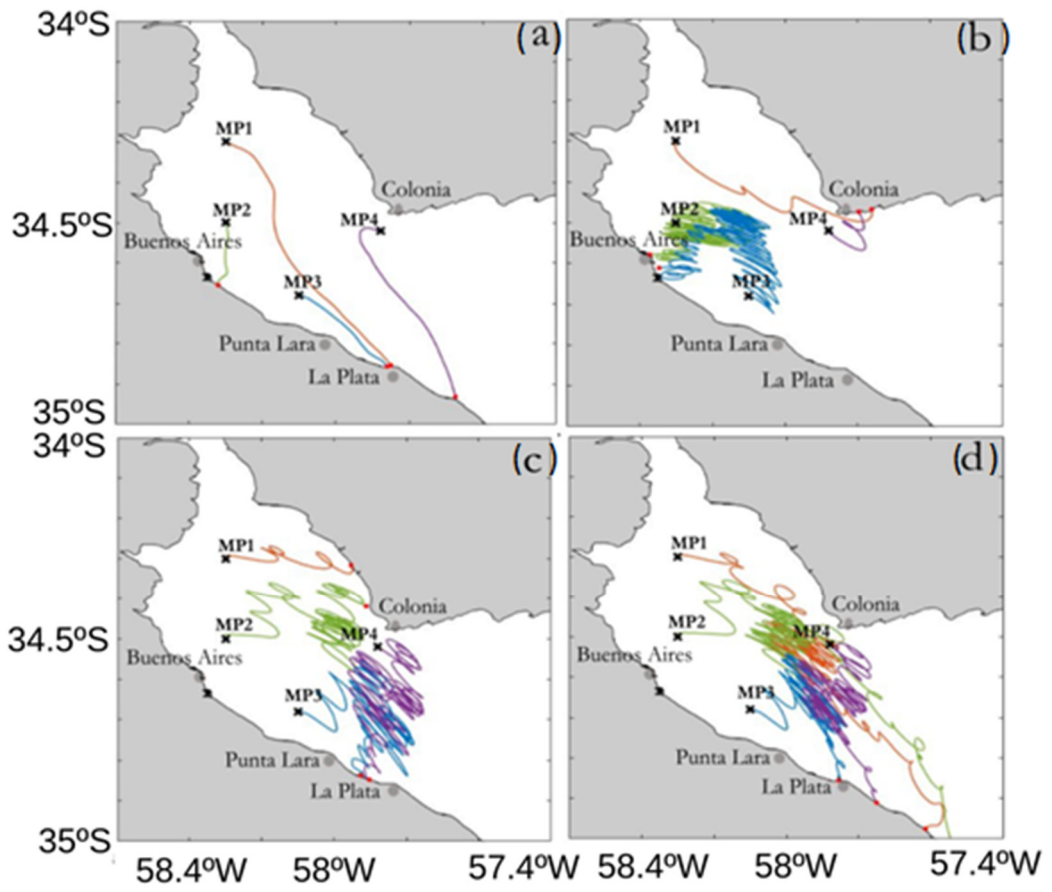

Figure 4. Trajectories of the four MPs: (**a**) continental discharge; (**b**) continental discharge + tides; (**c**) continental discharge + tides + winds; (**d**) discharge + tides + winds + waves. The "x" indicates the release location and the red dot indicates the final position. The resulting trajectories are colored orange for MP1, green for MP2, blue for MP3 and purple for MP4.

3.1.2. Hydrodynamic Case II: Effect of the Continental Discharge Plus Tides

The simulation was repeated by introducing tide in addition to the continental discharge for the same time period (Figure 4b). The outcomes for MP1 illustrate a trajectory that was notably impacted by the tributary discharge, yet exhibiting cyclical shifts attributed to the ebb and flow of tides. Consequently, MP1 reached the northern coast within a short span of time. In contrast, MP2 and MP3 displayed a classic tidal ebb-and-flow pattern in their movements, extending their permanence within the water for an extended duration. These MPs eventually arrived at the southern coast after approximately 528 h, near Buenos Aires city. Lastly, MP4's trajectory also underwent alterations, with its journey culminating near the city of Colonia de Sacramento.

3.1.3. Hydrodynamic Case III: Effect of the Continental Discharge Plus Tides Plus Winds

The simulation involved the addition of wind forcing to Case II (Figure 4c). MP1 displayed a predominantly easterly direction and a residence time of 54 h. Despite this, the trajectory was primarily impacted by the continental discharge, along with the northeasterly wind vectors observed during the initial days of November (as depicted in Figure 3). Nonetheless, the trajectory exhibited evident ebb-and-flow motions. For MP2, a residence time of 267 h was noted before it reached the Uruguayan coast. In the first 60 h, MP2 moved in a north-northeasterly direction. Subsequently, at 168 h, the movement shifted toward a south-southeasterly direction. Eventually, the trajectory changed course once more, moving northward until it reached the coast. MP3 and MP4 started their motion in a northerly direction under the influence of the wind, subsequently veering southwards until they

reached the coast. Both trajectories were influenced by the continental discharge and tide, generating periodic inward and outward movements within the RdP, albeit with an overall outward movement from the estuary. The wind significantly altered the trajectories of MP3 and MP4, distinctly deviating from the conditions of Case II. In this context, MP3 and MP4 remained within the estuary for 395 h and 365 h, respectively. The motion of these MPs also illuminated the impact of the wind pattern overlapping with tidal movement. Noticeably, a clear southeastwards net motion emerged (Figure 4c), attributed to wind stress vectors of approximately 5 N m^{-2} that appeared between the 48 and 72 h of that month.

3.1.4. Hydrodynamic Case IV: Effect of the Continental Discharge Plus Tides Plus Winds Plus Waves

The most complex and realistic simulation (Figure 4d) encompasses all the influencing factors of the system: continental discharge, tide, wind, and wind waves. MP1 and MP4, previously arriving at the Uruguayan coast in the hydrodynamic Case III, now make their way to the opposite coast, covering a larger distance that extends beyond the city of La Plata. MP2, however, continued to follow a south-southeasterly path, reaching the Argentinean (southern) coast and surpassing the distance traversed by the other MPs. In terms of motion, MP3 exhibited a path similar to its trajectory in the preceding hydrodynamic case (without wind waves), although it also covered a larger distance. Overall, the residence times for all MPs were extended in this simulation. MP1 remained in the water for approximately 400 h, whereas MP2, MP3, and MP4 spent around 165–167 h in the water before they eventually reached the coast. For these MPs, the complexity of their trajectories is evident, shaped by the ebb and flow of the tide, alongside displacements triggered by shifting wind directions. Additionally, the dynamics of locally generated waves induced by the wind played a role in influencing their paths.

3.1.5. Wind Dependence

To further understand the influence of wind on MPs trajectories, a dedicated investigation was conducted, initiating simulations under the three different wind strength and direction scenarios illustrated in Figure 3a. Figure 5a corresponds to W-I, the wind pattern with the highest variability and the longest simulation duration, resulting in the longest persistence of MPs in the water column. For MP1, the residence time was 400 h, while MP2, MP3, and MP4 had residence times of 167 h, 163 h, and 164 h, respectively. In this simulation, all four MPs traverse the vicinity of the city of La Plata and conclude their journey along the Argentine coast. Their motion aligns with the wind pattern: starting with a south-easterly motion, followed by a north-westerly shift midway through, and ultimately transitioning to a calmer trajectory toward the estuary's outward direction.

In W-II (Figure 5b), the impact of wind intensity on MP2 and MP4 becomes evident. These two MPs exhibit extended persistence in this simulation, initially moving southeastwards and then shifting to a northeast direction, eventually concluding their journeys north of their starting positions. MP1, however, is promptly influenced by the southeast direction, arriving at the coast above the Colonia city line. Regarding MP3, its trajectory cannot be fully appreciated due to its swift arrival at the coast. The residence times were MP1: 77 h, while MP2: 85 h, MP3: 13 h, and MP4: 102 h. Simulation W-III (Figure 5c), initialized on the 19th, represents a period with moderate winds. Here, the influences of other factors, such as continental inputs, become discernible on MP2 and MP3. Their trajectories are nearly linear, extending out of the estuary. Unexpectedly, MP1 displays a trajectory opposite to what was anticipated, moving northward. This discrepancy is likely a result of the combined effects of the discharge currents and the tides in the tributary inlet sector. Lastly, MP4 experiences the shortest trajectories, reaching the Uruguayan coast. In this situation, the retention time was 99 h for MP1, 59 h for MP2, 45 h for MP3, and 13 h for MP4.

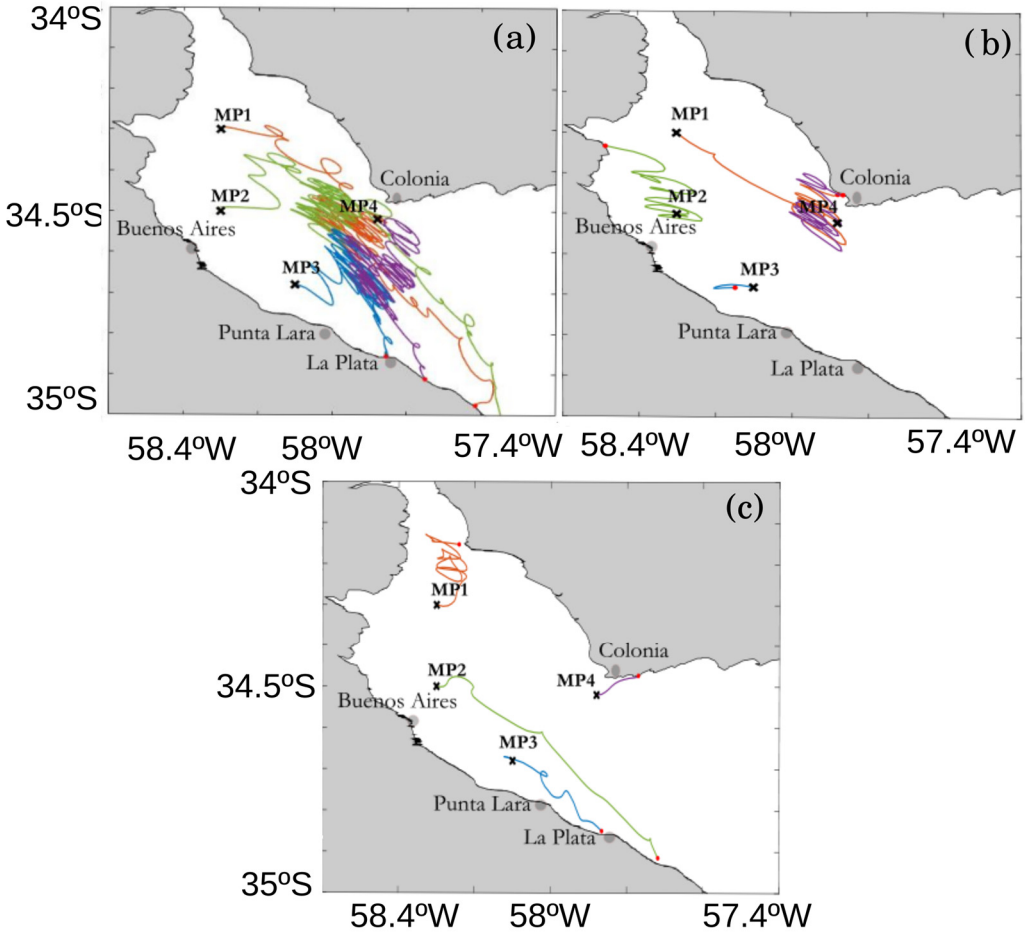

Figure 5. Upper panels: MP trajectories, (**a**) W-I releasing on the 1st, (**b**) case W-II releasing on the 7th, (**c**) W-III releasing on the 19th. The "x" indicates the release location and the red dot indicates the final position. The resulting trajectories are colored orange for MP1, green for MP2, blue for MP3 and purple for MP4.

3.2. Morphology Effects

As previously mentioned, two different geometries were examined under Case IV, considering PS spheres and cylindrical tubes in two distinct sizes. For spheres, radii of 150 µm and 10 µm were chosen, while for cylinders, radii of 150 µm with a length of 3000 µm, and 10 µm with a length of 200 µm were selected. Each one has a particular settling velocity determined by Equations (4) and (5). But the vertical displacement (Equation (2)) also depends on the vertical velocity (w) and the vertical diffusion coefficient (Equation (3)).

Figure 6a shows the vertical motion in longitude, while Figure 6b shows the vertical motion in latitude, with a cylinder morphology of 150 and 3000 µm, a fiber morphology of 10 and 200 µm, a sphere morphology of 150 µm and a sphere morphology of 10 µm, and the MPs used in behavior B1 are those with buoyant trajectories. The trajectories shown in Figure 6a,b correspond to MP3, and the general behavior of MP1, MP2, and MP4 is similar. In both figures, larger morphologies with a radius of 150 µm reached the bottom of the estuary in less than 2 h with overlapping trajectories. On the contrary, smaller morphologies increase their persistence in the estuarine water column. The smaller spheres have a settling velocity of 0.5×10^{-5} m s^{-1} and remain in the estuary for almost 150 h. Figure 6a,b show that this particular size of sphere behaves similarly to a positively buoyant particle. This vertical movement also revealed the influence of the hydrodynamics of the system, manifested as ebb and flow due to tidal effects. The cylinder with the same radius, 10 µm, has a settling velocity of 1.98×10^{-5} m s^{-1} and took 48 h to reach the bottom, showing movements less influenced by hydrodynamic forces. On the other hand, the

buoyant microplastic never reaches the bottom during the month of simulation, remaining in the first layer of the estuary, with trajectories strongly influenced by the hydrodynamics of the RdP.

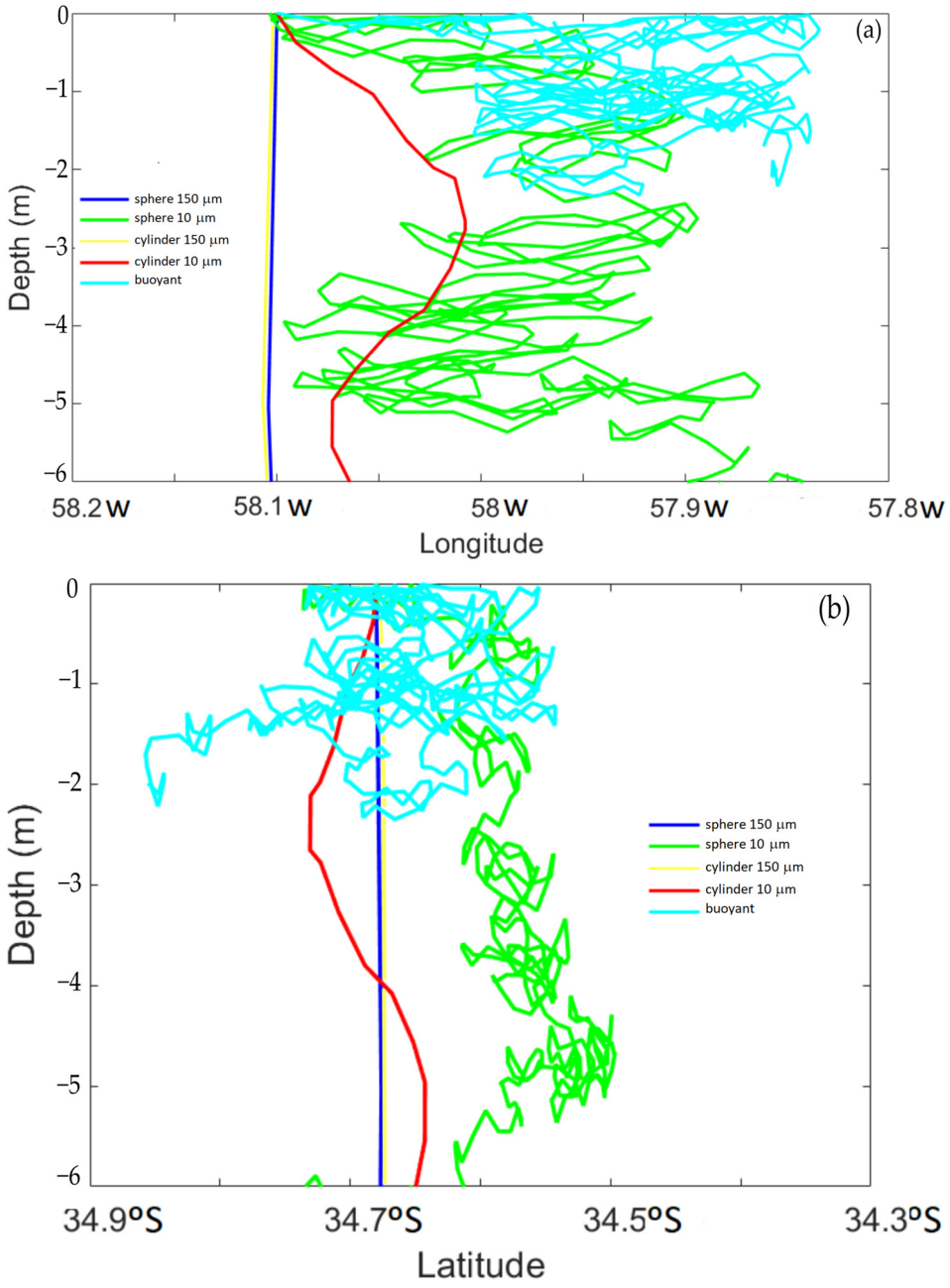

Figure 6. (**a**) Vertical motion for MP3 in longitude, (**b**) vertical motion for MP3 in latitude. Both with morphology of sphere 150 µm (blue), sphere 10 µm (green), cylinder 150–3000 µm (yellow), and cylinder 10–200 µm (red), buoyant (cyan).

4. Discussion

Throughout the analysis of the hydrodynamics simulations, a robust correlation between the hydrodynamics of the RdP and the trajectories of positively buoyant MPs becomes evident. This correlation is in line with the investigation into various influencing factors, continental discharge, the flood and ebb tidal cycle, and its tidal range (spring/neap) and wind effect [63].

MPs positioned in both the upper and intermediate regions of the RdP displayed paths in alignment with the barotropic circulation patterns of the upper estuary. In particular, MPs near the mouths of tributaries displayed trajectories largely influenced by the force of continental discharge, while those situated near the southern shore of the upper RdP exhibited ebb-and-flow movements that corresponded to the tidal patterns. This observation aligns with the findings of Lentz and Fewings (2012) [64], who previously discussed the complex circulation responsible for MPs transport. The simulation process highlighted that the circulation patterns of inner estuarine regions are more influenced by the wind direction than by its strength, characterized by a rapid response time of the currents ranging from 3 to 9 h [41]. This wind dependency underscores the significant correlation between the prevailing wind conditions during the analyzed period and the dynamics of positively buoyant MPs, as corroborated by Díez-Minguito et al. (2020) [65] and Van Sebille et al. (2020) [12], who found that the distribution and movement of MPs in the estuary were mainly influenced by wind forcing, which had a greater impact on circulation compared to density-driven and river flows. Finally, the random effect is included in the model (Equation (1)), modifying the final destination of microplastics, but it needs a more in-depth study to analyze this effect.

The motion within the water column for a particle is governed by its settling velocity (w_s), wherein larger sizes result in higher fall velocities [66]. The work of Jalón-Rojas et al. (2019) [24] demonstrated that simulated MPs, particularly those of larger sizes, tended to settle close to their initial release point, leading to shorter horizontal trajectories. A positive relationship between diameter and w_s was also noted by Katmullina and Isachinko (2017) [14], who observed accelerated settling velocities with increasing diameter under laboratory conditions with static fluids. Smaller particles were also observed to have longer residence times than larger particles, which is consistent with the observations of Elagani et al. (2017) [67], who found that the mean residence time of the smallest microplastic particles (1–30 μm) was orders of magnitude higher than the larger ones (100–1000 μm). As the settling velocity of MPs under laminar conditions depends on their weight and buoyancy forces, all large and dense particles have significantly higher settling velocities than the smaller and lighter microplastics [67]. The 10 μm spheres showed vertical motions more similar to buoyant particles, clearly influenced by the effects of estuarine turbulence. So the behavior of the MPs seems to be more influenced by the size than by the density of the microplastic. Given the high concentration of sediments in the RdP, even in the barotropic zones of the estuary, it would be interesting to study their behavior, taking into account flocculation effects. Studies have shown that positively buoyant microplastics of small size flocculate and settle with natural fine-grained suspended sediment (<20 μm) in river and estuarine waters [68].

5. Conclusions

Numerical models capable of reliably predicting the movement and behavior of MP particles in water are invaluable tools for identifying pathways, potential sources, and hotspots. In this research, we have taken a first step by applying two numerical models to investigate the trajectories of MPs in the RdP estuary. This effort represents an important first step to understanding the motion of these emerging contaminants in this complex environment. The simulation results have provided important insights into how the hydrodynamics of the RdP predominantly dictate the trajectories of MPs. Our results show that the horizontal movement of MPs is primarily influenced by tidal effects, whereas wind and wave patterns have a significant impact. In particular, near the water surface, wind direction and intensity play a crucial role in determining the main trajectory of MPs. The continental discharge has more influence on the microplastics released near the tributary mouth. In addition, the inherent characteristics of MPs—such as their type, morphology, density, and size—strongly influence their behavior. Larger or denser MPs quickly sink, whereas lighter and smaller particles tend to remain suspended. As this study represents an initial exploration in understanding the motion of MPs within the RdP, there are several

alternatives for further investigation. They include exploring alternative microplastic behaviors, extending the length of simulations, investigating the dynamics of vertical motion, and considering scenarios of continuous microplastic release over time to analyze the random effect. Moreover, we propose initiating the collection of field samples to validate the characteristics and types of the selected MPs. In sum, the outcomes of this research contribute to crucial foundational knowledge in the field of MPs movement dynamics within estuarine environments. By enhancing our understanding of the complex interplay between hydrodynamics, particle properties, and external influences, we will be able to develop more accurate predictive models and strategies for managing the environmental impact of MPs pollution.

Author Contributions: Conceptualization, A.E.S., D.M.; methodology, A.E.S., D.M.; formal analysis, A.E.S., D.M.; investigation, A.E.S., D.M.; writing—original draft preparation, A.E.S., D.M.; writing—review and editing, A.E.S., D.M.; supervision, P.E., C.G.S.; project administration, D.M. All authors have read and agreed to the published version of the manuscript.

Funding: This study was funded by the National Agency for Scientific and Technological Research of Argentina (ANPCyT, PICT 2020 Serie A-1879), the National Council for Scientific and Technological Research of Argentina (CONICET, PIBAA 2022-2023, R73732), the University of Buenos Aires (UBA, UBACYT 20020220400151BA), and the National Institute of Industrial Technology (INTI).

Institutional Review Board Statement: Not applicable.

Informed Consent Statement: Not applicable.

Data Availability Statement: The data and results presented are available and can be requested by mail to the author. "Sistema Nacional de Información Hídrica de la Nación": https://snih.hidricosargentina.gob.ar/ (accessed on 20 November 2023). TrackMPD: https://isabeljalonrojas.com/trackmpd/ (accessed on 20 November 2023).

Conflicts of Interest: The authors declare no conflict of interest.

References

1. Kane, I.A.; Clare, M.A.; Hodgson, D.M.; Kane, I.A. Dispersion, Accumulation, and the Ultimate Fate of Microplastics in Deep-Marine Environments: A Review and Future Directions. *Front. Earth Sci.* **2019**, *7*, 80. [CrossRef]
2. Petersen, F.; Hubbart, J.A. The Occurrence and Transport of Microplastics: The State of the Science. *Sci. Total Environ.* **2021**, *758*, 143936. [CrossRef] [PubMed]
3. He, J.; Yang, X.; Liu, H. Enhanced Toxicity of Triphenyl Phosphate to Zebrafish in the Presence of Micro- and Nano-Plastics. *Sci. Total Environ.* **2021**, *756*, 143986. [CrossRef] [PubMed]
4. Bermúdez, M.; Vilas, C.; Quintana, R.; Gonzales-Fernandez, D.; Cózar, A.; Diez-Minguito, M. Unravelling Spatio-Temporal Patterns of Suspended Microplastic Concentration in the Natura 2000 Guadalquivir Estuary (SW Spain): Observations and Model Simulations. *Mar. Pollut. Bull.* **2021**, *170*, 112622. [CrossRef] [PubMed]
5. Geyer, R.; Jambeck, J.R.; Law, K.L. Production, Use, and Fate of All Plastics Ever Made. *Sci. Adv.* **2017**, *3*, 25–29. [CrossRef]
6. Luo, W.; Su, L.; Craig, N.J.; Du, F.; Wu, C.; Shi, H.A.C. Comparison of microplastic pollution in different water bodies from urban creeks to coastal waters. *Environ. Pollut.* **2018**, *246*, 174–182. [CrossRef] [PubMed]
7. Chen, X.; Chen, X.; Zhao, Y.; Zhou, H.; Xiong, X.; Wu, C. Effects of Microplastic Biofilms on Nutrient Cycling in Simulated Freshwater Systems. *Sci. Total. Environ.* **2020**, *719*, 137276. [CrossRef]
8. Tursi, A.; Baratta, M.F.; Easton, T.; Chatzisymeon, E.; Chidichimo, F.; De Biase, M.; De Filpo, G. Microplastics in Aquatic Systems, a Comprehensive Review: Origination, Accumulation, Impact, and Removal Technologies. *R. Soc. Chem.* **2022**, *12*, 28318–28340. [CrossRef]
9. Isobe, A.; Uchiyama-Matsumoto, K.; Uchida, K.; Tokai, T. Microplastics in the Southern Ocean. *Mar. Pollut. Bull.* **2017**, *114*, 623–626. [CrossRef]
10. Lu, H.C.; Ziajahromi, S.; Neale, P.A.; Leusch, F.D.L. A Systematic Review of Freshwater Microplastics in Water and Sediments: Recommendations for Harmonisation to Enhance Future Study Comparisons. *Sci. Total Environ.* **2021**, *781*, 146693. [CrossRef]
11. Bom, F.C.; Sá, F. Concentration of Microplastics in Bivalves of the Environment: A Systematic Review. *Environ. Monit. Assess.* **2021**, *193*, 1–30. [CrossRef] [PubMed]
12. Van Sebille, E.; Aliani, S.; Law, K.L.; Maximenko, N.; Alsina, J.M.; Bagaev, A.; Bergmann, M.; Chapron, B.; Chubarenko, I.; Cózar, A.; et al. The Physical Oceanography of the Transport of Floating Marine Debris. *Environ. Res. Lett.* **2020**, *15*, 023003. [CrossRef]

13. Larsen, B.E.; Al-Obaidi, M.A.A.; Guler, H.G.; Carstensen, S.; Goral, K.D.; Christensen, E.D.; Kerpen, N.B.; Schlurmann, T.; Fuhrman, D.R. Experimental Investigation on the Nearshore Transport of Buoyant Microplastic Particles. *Mar. Pollut. Bull.* **2023**, *187*, 114610. [CrossRef] [PubMed]
14. Khatmullina, L.; Chubarenko, I. Transport of Marine Microplastic Particles: Why Is It so Difficult to Predict? *Anthr. Coasts* **2019**, *2*, 293–305. [CrossRef]
15. Hardesty, B.D.; Harari, J.; Isobe, A.; Lebreton, L.; Maximenko, N.; Potemra, J.; Sebille, E.V.; Vethaak, A.D.; Wilcox, C. Using Numerical Model Simulations to Improve the Understanding of Micro-Plastic Distribution and Pathways in the Marine Environment. *Front. Mar. Sci.* **2017**, *4*, 1–9. [CrossRef]
16. Lebreton, L.; Slat, B.; Ferrari, F.; Sainte-Rose, B.; Aitken, J.; Marthouse, R.; Hajbane, S.; Cunsolo, S.; Schwarz, A.; Levivier, A.; et al. Evidence That the Great Pacific Garbage Patch Is Rapidly Accumulating Plastic. *Sci. Rep.* **2018**, *8*, 4666. [CrossRef]
17. Neumann, D.; Callies, U.; Matthies, M. Marine Litter Ensemble Transport Simulations in the Southern North Sea. *Mar. Pollut. Bull.* **2014**, *86*, 219–228. [CrossRef]
18. Critchell, K.; Grech, A.; Schlaefer, J.; Andutta, F.P.; Lambrechts, J.; Wolanski, E.; Hamann, M. Modelling the Fate of Marine Debris along a Complex Shoreline: Lessons from the Great Barrier Reef. *Estuar. Coast. Shelf Sci.* **2015**, *167*, 414–426. [CrossRef]
19. Liubartseva, S.; Coppini, G.; Lecci, R.; Creti, S. Regional Approach to Modeling the Transport of Floating Plastic Debris in the Adriatic Sea. *Mar. Pollut. Bull.* **2016**, *103*, 115–127. [CrossRef]
20. Carlson, D.F.; Suaria, G.; Aliani, S.; Fredj, E.; Fortibuoni, T.; Griffa, A.; Russo, A.; Melli, V. Combining Litter Observations with a Regional Ocean Model to Identify Sources and Sinks of Floating Debris in a Semi-Enclosed Basin: The Adriatic Sea. *Front. Mar. Sci.* **2017**, *4*, 78. [CrossRef]
21. Alsina, J.M.; Jongedijk, C.E.; van Sebille, E. Laboratory Measurements of the Wave-Induced Motion of Plastic Particles: Influence of Wave Period, Plastic Size and Plastic Density. *J. Geophys. Res. Oceans* **2020**, *125*, e2020JC016294. [CrossRef] [PubMed]
22. Guler, H.G.; Larsen, B.E.; Quintana, O.; Goral, K.D.; Carstensen, S.; Christensen, E.D.; Kerpen, N.B.; Schlurmann, T.; Fuhrman, D.R. Experimental Study of Non-Buoyant Microplastic Transport beneath Breaking Irregular Waves on a Live Sediment Bed. *Mar. Pollut. Bull.* **2022**, *181*, 113902. [CrossRef] [PubMed]
23. Passalacqua, G.; Iuppa, C.; Faraci, C. A Simplified Experimental Method to Estimate the Transport of Non-Buoyant Plastic Particles Due to Waves by 2D Image Processing. *J. Mar. Sci. Eng.* **2023**, *11*, 1599. [CrossRef]
24. Jalón-Rojas, I.; Wang, X.H.; Fredj, E. A 3D Numerical Model to Track Marine Plastic Debris (TrackMPD): Sensitivity of Microplastic Trajectories and Fates to Particle Dynamical Properties and Physical Processes. *Mar. Pollut. Bull.* **2019**, *141*, 256–272. [CrossRef]
25. Cheng, M.L.H.; Lippmann, T.C.; Dijkstra, J.A.; Bradt, G.; Cook, S.; Choi, J.; Brown, B.L. A Baseline for Microplastic Particle Occurrence and Distribution in Great Bay Estuary. *Mar. Pollut. Bull.* **2021**, *170*, 112653. [CrossRef] [PubMed]
26. Siegfried, M.; Koelmans, A.A.; Besseling, E.; Kroeze, C. Export of Microplastics from Land to Sea. A Modelling Approach. *Water Res.* **2017**, *127*, 249–257. [CrossRef]
27. Carreto, J.I.; Montoya, N.G.; Akselman, R.; Roja, P.M. Proyecto "Protección Ambiental del Río de la Plata y su Frente Marítimo: Prevención y Control de la Contaminación y Restauración de Hábitats". *RLA* **2004**, *99*, G31.
28. Simionato, C.G.; Vera, C.S.; Siegismund, F.; Beach, W.P.; Simionato, C.G.; Vera, C.S.; Siegismund, F. Surface Wind Variability on Seasonal and Interannual Scales Over Río de La Plata Area Surface Wind Variability on Seasonal and Interannual Scales Over Rı ´ o de La Plata Area. *J. Coast. Res.* **2005**, *214*, 770–783. [CrossRef]
29. Pazos, R.S.; Amalvy, J.; Pecile, A.; Cochero, J.; Gomez, N. Temporal Patterns in the Abundance, Type and Composition of Microplastics on the Coast of the Río de La Plata Estuary. *Mar. Pollut. Bull.* **2021**, *168*, 112382. [CrossRef]
30. Arias, A.H.; Ronda, A.C.; Oliva, A.L.; Marcovecchio, J.E. Evidence of Microplastic Ingestion by Fish from the Bahía Blanca Estuary in Argentina, South America. *Bull. Environ. Contam. Toxicol.* **2019**, *102*, 750–756. [CrossRef]
31. Balay, M.A. El Río de La Plata Entre La Atmósfera y El Mar. *H-621 B. Aires Serv. Hidrogr. Nav. Armada Argent.* **1961**, *153*.
32. Borús, J.; Giacosa, J. Evaluación de Caudales Diarios Descargados Por Los Grandes Ríos Del Sistema Del Plata al Río de La Plata. In *Direccion y Alerta Hidrológico*; Instituto Nacional del Agua: Ezeiza, Argentina, 2014.
33. Borús, J.; Uriburu Quirno, M.; Calvo, D. *Evaluación de Caudales Diarios Descargados 470 Por Los Grandes Ríos del Sistema del Plata al Estuario del Río de la Plata, Dirección de Sistemas de Información y Alerta Hidrológico*; Instituto Nacional del Agua: Ezeiza, Argentina, 2017.
34. Simionato, C.G. Estudio de La Dinámica Hidro-Sedimentológica-Del Río de La Plata. *Proyecto FREPLATA* **2011**, *99*, G31.
35. Ottoman, F.; Urien, C.M. Sur Quelques Problemes Sedimentologiques Dans Le Río de La Plata. *Rev. Géographie Phys. Géologie Dyn.* **1996**, 209–224.
36. Parker, G.; Cavalloto, J.L.; Marcolini, S.; Violante, R. *Los Registros Acústicos en la Diferenciación de Sedimentos Subácueos Actuales (Río de La Plata)*; 1986; pp. 32–44.
37. Siomionato, C.G.; Meccia, V.L.; Guerrero, R.A.; Dragani, W.C.; Nuñez, M.N. The Río de La Plata Estuary Response to Wind Variability in Synoptic to Intra-Seasonal Scales: II Currents Vertical Structure and Its Implications on the Salt Wedge Structure. *J. Geophys. Res. Oceans* **2007**, *112*, C07005. [CrossRef]
38. Simionato, C.G.; Dragani, W.C.; Nuñez, M.N.; Engel, M. A Set of 3-D Nested Models for Tidal Propagation from the Argentinean Continental Shelf to the Río de La Plata Estuary—Part I M2. *J. Coast. Res.* **2004**, *20*, 893–912. [CrossRef]
39. Guerrero, R.A.; Acha, E.M.; Framiñan, M.B.; Lasta, C. Physical Oceanography of the Río de La Plata Estuary, Argentina. *Cont. Shelf Res.* **1997**, *17*, 727–742. [CrossRef]

40. Meccia, V.L.; Simionato, C.G.; Guerrero, R.A. The Río de la plata estuary response to wind variability in synoptic timescale: Salinity fields and salt wedge structure. *J. Coast. Res.* **2013**, *29*, 61–77. [CrossRef]
41. Simionato, C.; Dragani, W.C.; Meccia, V.L.; Nuñez, M.N. A Numerical Study of the Barotropic Circulation of the Río de La Plata Estuary: Sensitivity to Bathymetry, Earth Rotation and Low Frequency Wind Variability. *Estuar. Coast. Shelf Sci.* **2004**, *61*, 261–273. [CrossRef]
42. Jaime, P.R.; Menéndez, Á.N. Vinculación Entre ElCaudal Del Río Paraná yEl Fenómeno de El Niño. Instituto Nacional del Agua. 2003. Available online: https://repositorio.ina.gob.ar/handle/123456789/462 (accessed on 20 November 2023).
43. Jaime, P.R.; Menéndez, Á.N. Modelo Hidrodinámico "Ríode La Plata 2000". Report LHA-INA 183-01-99, INA. 1999. Available online: https://repositorio.ina.gob.ar/handle/123456789/92 (accessed on 20 November 2023).
44. Magni, L.F.; Castro, L.N.; Rendina, A.E. Evaluation of Heavy Metal Contamination Levels in River Sediments and Their Risk to Human Health in Urban Areas: A Case Study in the Matanza-Riachuelo Basin, Agentina. *Environ. Res.* **2021**, *197*, 110979. [CrossRef]
45. O'Farrell, I.; Lombardo, R.; Tezanos, P.; Loez, C. The Assessment of Water Quality in the Lower Luján River (Buenos Aires, Argentina): Phytoplankton and Algal Bioassay. *Environ. Pollut.* **2002**, *20*, 207–218. [CrossRef]
46. Moreira, D.; Simionato, C.G. Modeling the Suspended Sediment Transport in a Very Wide, Shallow, and Microtidal Estuary, the Río de La Plata, Argentina. *J. Adv. Model. Earth Syst.* **2019**, *11*, 3284–3304. [CrossRef]
47. Minetti, J.L.; Vargas, W.M. Comportamiento Del Borde Antiticiclónico Subtropical En Sudamérica. *Rev. Geofísica* **1990**, 177–190.
48. Simionato, C.; Meccia, V.L.; Dragani, W.C.; Nuñez, M.N. On the Use of the NCEP/NCAR Surface Winds for Modeling Barotropic Circulation in the Río de La Plata Estuary. *Estuar. Coast. Shelf Sci.* **2006**, *70*, 195–206. [CrossRef]
49. Vera, C.S.; Vigliarolo, P.K.; Berbery, E.H. Cold Season Synoptic Scale Waves over Subtropical South America. *Mon. Weather Rev.* **2002**, *130*, 684–699. [CrossRef]
50. Dragani, W.C.; Romero, S.I. Impact of a Possible Local Wind Change on the Wave Climate in the Upper Río de La Plata. *Int. J. Climatol.* **2004**, *24*, 1149–1157. [CrossRef]
51. Lazure, P.; Dumas, F. An External-Internal Mode Coupling for a 3D Hydrodynamical Model for Applications at Regional Scale (MARS). *Adv. Water Resour.* **2008**, *31*, 233–250. [CrossRef]
52. Lazure, P.; Salomon, J.C. Coupled 2-D and 3-D Modelling of Coastal Hydrodynamics. *Oceanol. Acta* **1991**, *14*, 173–180.
53. Andre, G.; Garreau, P.; Garnier, V.; Fraunié, P. Modelled Variability of the Sea Surface Circulation in the North-Western Mediterranean Sea and in the Gulf of Lions. *Ocean Dyn.* **2005**, *55*, 294–308. [CrossRef]
54. Pous, S. Dynamique Océanique Dans Les Golfes Persique et d'Oman, Phdthesis, Université de Bretagne Occidentale. 2005. Available online: https://theses.hal.science/tel-01301686 (accessed on 20 November 2023).
55. Fossati, M.; Piedra-Cueva, I. A 3D Hydrodynamic Numerical Model of the Río de La Plata and Montevideo's Coastal Zone. *Appl. Math. Model.* **2013**, *37*, 1310–1332. [CrossRef]
56. Moreira, D. Estudio de Los Procesos Que Determinan El Transporte de Los Sedimentos Finos y Su Variabilidad En El Río de La Plata En Base a Simulaciones Numéricas y Observaciones Satelitales e in Situ. Phdthesis Universidad de Buenos Aires, Facultad de Ciencias Exactas y Naturales, Buenos Aires, Argentina. 2016. Available online: https://hdl.handle.net/20.500.12110/tesis_n6101_Moreira (accessed on 20 November 2023).
57. Simionato, C.; Meccia, V.L.; Dragani, W.C. On the Path of Plumes of the Río de La Plata Estuary Main Tributaries and Their Mixing Scales. *GEOACTA* **2009**, *34*, 87–116.
58. Jaime, P. Analisis Del Regimen Hidrologico de Los Rios Parana y Uruguay. *Prot. Ambient. Rio Plata Su Frente Maritimo Prev. Control Contam. Restaur. Habitats* **2002**, *53*, 160.
59. Enders, K.; Lenz, R.; Stedmon, C.A.; Nielsen, T.G. Abundance, Size and Polymer Composition of Marine Microplastics ≥10 Mm in the Atlantic Ocean and Their Modelled Vertical Distribution. *Mar. Pollut. Bull.* **2015**, *100*, 70–81. [CrossRef] [PubMed]
60. Plastic Europe. Plastics—The Facts 2019. Plastics Europe AISBL. Brussel, Belgium. 2019. Available online: https://plasticseurope.org/wp-content/uploads/2021/10/2019-Plastics-the-facts.pd. (accessed on 20 November 2023).
61. Rodrigues, S.M.; Almeida, C.M.R.; Silva, D.; Cunha, J.; Antunes, C.; Freitas, V.; Ramos, S. Science of the Total Environment Microplastic Contamination in an Urban Estuary: Abundance and Distribution of Microplastics and Fi Sh Larvae in the Douro Estuary. *Sci. Total Environ.* **2019**, *659*, 1071–1081. [CrossRef]
62. Moreira, D.; Simionato, C.; Re, M.; Gerbec, M.S.; Cayocca, F.; Fossati, M. Implementación de Un Modelo Numérico Para El Estudio Del Transporte de Sedimentos Finos En El Río de La Plata. In Proceedings of the IFRH 2012-Primer Encuentro de Investigadores en Formación en Recursos Hídricos, Buenos Aires, Argentina, 14–15 June 2012.
63. Feng, Q.; An, C.; Chen, Z.; Lee, K.; Zheng, W. Identification of the Driving Factors of Microplastic Load and Morphology in Estuaries for Improving Monitoring and Management Strategies: A Global Meta-Analysis. *Environ. Pollut.* **2023**, *333*, 122014. [CrossRef] [PubMed]
64. Lentz, S.; Fewings, M.R. The Wind- and Wave-Driven Inner-Shelf Circulation. *Annu. Rev. Mar. Sci.* **2012**, *4*, 317–343. [CrossRef] [PubMed]
65. Diez-Minguito, M.; Bermúdez, M.; Gago, J.; Carretero, O.; Viña, L. Observations and Idealized Modelling of Microplastic Transport in Estuaries: The Exemplary Case of an Upwelling System (Ría de Vigo, NW Spain). *Mar. Chem.* **2020**, *222*, 103780. [CrossRef]

66. Lawrence, C.; Neff, J. The Contemporary Physical and Chemical Flux of Aeolian Dust: A Synthesis of Direct Measurements of Dust Deposition. *Chem. Geol.* **2009**, *267*, 46–63. [CrossRef]
67. Elagami, H.; Ahmadi, P.; Fleckenstein, J.H.; Frei, S.; Obst, M.; Agarwal, S.; Gilfedder, B.S. Measurement of Microplastic Settling Velocities and Implications for Residence Times in Thermally Stratified Lakes. *Limnol. Oceanogr.* **2022**, *67*, 934–945. [CrossRef]
68. Laursen, S.N.; Fruergaard, M.; Dodhia, M.S.; Posth, N.R.; Rasmussen, M.B.; Larsen, M.N.; Shilla, D.; Shilla, D.; Kilawe, J.J.; Kizenga, H.J.; et al. Settling of Buoyant Microplastic in Estuaries: The Importance of Flocculation. *Sci. Total Environ.* **2023**, *886*, 163976. [CrossRef]